Journal of Materials Chemistry B

ROYAL SOCIETY OF CHEMISTRY

COMMUNICATION

View Article Online
View Journal

Check for updates

Cite this: DOI: 10.1039/d5tb01244a

Received 23rd May 2025,
Accepted 8th December 2025

DOI: 10.1039/d5tb01244a

rsc.li/materials-b

Continuous electrochemical H_2O_2 delivery for cancer cell treatment

Marie Jakešová, *[a] Jiří Ehlich,[a] Sabine Erschen,[bc] Leia Nemeskeri,[b] Verena Handl,[bc] Linda Waldherr *[bc] and Eric D. Głowacki [a]

Hydrogen peroxide (H_2O_2) has emerged as a promising agent in cancer therapy due to its ability to induce oxidative stress selectively in tumor cells, however, its efficacy is severely hampered by H_2O_2 breakdown when administered *via* standard routes. Our study introduces an innovative electrochemical method for the controlled and continuous delivery of H_2O_2 directly to cancer cells, potentially enhancing the efficacy of cancer treatments. We investigated the performance of gold, titanium, stainless steel, and poly(3,4-ethylenedioxythiophene), PEDOT, electrodes in generating H_2O_2, with PEDOT exhibiting superior consistency and efficiency in cell culture medium. The galvanostatic delivery of H_2O_2 demonstrated a dose-dependent reduction in cell viability for U87 glioblastoma and A375 melanoma cells, confirming the cytotoxic impact of H_2O_2. The addition of catalase restored cell viability, further validating the specificity of H_2O_2-induced cell death. Our results showed that U87 cells exhibited higher resistance to H_2O_2 compared to A375 cells, aligning with known tumor-specific variations in H_2O_2 metabolism. This novel approach of electrochemical H_2O_2 delivery holds significant potential for enhancing targeted cancer therapies, offering a controllable, precise, and efficient method for inducing tumor cell death while minimizing damage to healthy tissues. These results showcase the remarkable ability of PEDOT electrodes as a reliable electrocatalytic source of on-demand H_2O_2 in electrochemically-challenging biological environments.

Open Access Article. Published on 09 December 2025. Downloaded on 1/18/2026 3:46:00 AM.
This article is licensed under a Creative Commons Attribution 3.0 Unported Licence.

1. Introduction

Cancer remains one of the most formidable challenges in modern medicine. Despite significant progress in chemotherapy, immunotherapy, radiation therapy, and surgery, many of these treatments remain invasive, systemic, and limited by side effects and varying efficacy. Therefore, there is a pressing need to explore alternative therapeutic approaches that can enhance treatment outcomes while minimizing adverse effects. Hydrogen peroxide (H_2O_2) has emerged as a promising therapeutic agent due to its capacity to induce cell death in a dose-dependent manner.[1–6] Naturally-occurring H_2O_2 plays crucial roles in cellular signaling and immune responses,[7] but when administered exogenously, it induces various cellular responses depending on its concentration.[8] Low concentrations may promote proliferation, moderate levels induce temporary growth arrest and activate stress responses, while high concentrations can lead to cell death such as apoptosis, ferroptosis, and necrosis.[1,8–10] Unlike other reactive oxygen species (ROS), H_2O_2 can accumulate to pharmacologically relevant concentrations due to its relatively slow decomposition kinetics, making it a molecule of growing interest in redox-based cancer therapy.[1,11]

The selectivity of H_2O_2 toward cancer cells arises from their distinct metabolic and redox profiles. Tumor cells frequently exhibit mitochondrial dysfunction, elevated basal ROS, and an increased labile iron pool, promoting Fenton-type reactions that yield highly toxic hydroxyl radicals.[12–16] Moreover, many tumors display diminished activity of key detoxifying enzymes such as catalase (Cat) and glutathione peroxidase (GPx), which limits their ability to neutralize peroxide and enhances their susceptibility to oxidative damage.[13,17] Given the known variability in H_2O_2 sensitivity among cancer types,[17] the therapeutic effect of peroxide-based treatments will strongly depend on the cellular redox phenotype. This underlines the need for platforms that can precisely control both the concentration and exposure time of H_2O_2, enabling systematic studies across different cell types and redox states.

Despite the promising *in vitro* evidence, maintaining relevant peroxide concentrations in biological systems remains a fundamental challenge. Rapid enzymatic and non-enzymatic degradation prevents continuous exposure of cancer cells to effective doses.[18] Even in *in vitro* tests, where H_2O_2 is typically pipetted into the medium, its concentration decays rapidly (Fig. 1(a) and (b)).

[a] *Bioelectronics Materials and Devices Laboratory, Central European Institute of Technology, Brno University of Technology, Purkyňova 123, Brno 61200, Czech Republic. E-mail: jakesova@vutbr.cz*
[b] *Gottfried Schatz Research Center, Division of Medical Physics and Biophysics, Medical University of Graz, Austria*
[c] *BioTechMed-Graz, Austria, Auenbruggerplatz 30, 8036 Graz, Austria. E-mail: linda.waldherr@medunigraz.at*

Open Access Article. Published on 09 December 2025. Downloaded on 1/18/2026 3:46:00 AM.
This article is licensed under a Creative Commons Attribution 3.0 Unported Licence.

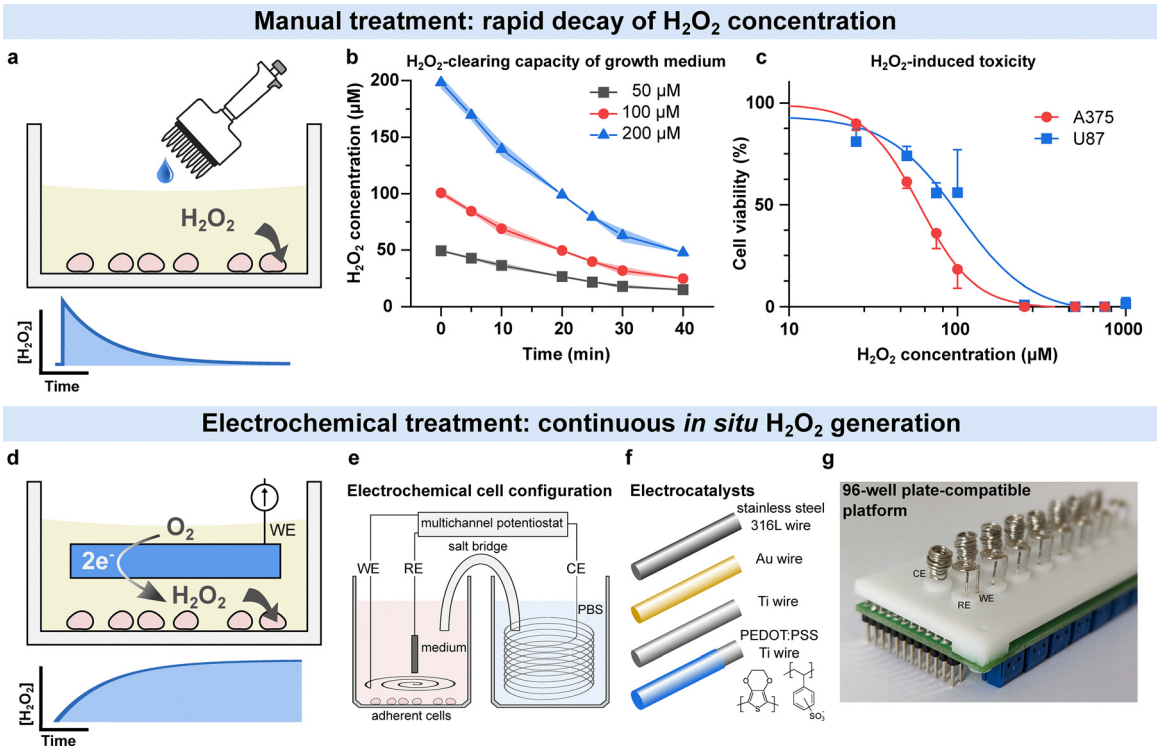

Fig. 1 Comparison of manual and electrochemical H_2O_2 treatments *in vitro*. (a)–(c) Experimental results for manual H_2O_2 addition to cell culture medium: (a) schematic of bolus application and decay profile, (b) time-dependent H_2O_2 clearance in growth medium supplemented with active FBS (n = 2–4), and (c) H_2O_2-induced cytotoxicity in A375 and U87 cells (n = 4). (d)–(g) Experimental setup enabling continuous electrochemical H_2O_2 production: (d) schematic of cathodic two-electron oxygen reduction on the working electrode, (e) schematic of a single electrochemical cell used for *in situ* H_2O_2 generation, with growth medium containing adherent cells and a PBS counter electrolyte chamber connected *via* a salt bridge; up to eight such cells can be operated in parallel using a multichannel potentiostat, (f) electrode materials evaluated, and (g) custom multichannel well-plate-compatible platform. (CE = counter electrode, WE = working electrode, RE = reference electrode).

Achieving sustained, spatially localized H_2O_2 exposure is therefore a prerequisite for meaningful biological and translational research. Several approaches have been developed to address this limitation. These include controlled release from vesicles, enzymatic generation using oxidases (*e.g.*, glucose or lactate oxidase) that simultaneously deplete key metabolites, and administration of pro-oxidant molecules that yield H_2O_2 *via* autooxidation, redox cycling, or metal-ion interactions.[15,19,20] For example, a current clinical approach using H_2O_2 as an anti-tumor agent features a high-dose ascorbate as a pro-drug, which is metabolized *via* ascorbate radicals to H_2O_2.[21,22] While these methods demonstrate the therapeutic potential of peroxide, they often lack temporal and spatial control and are difficult to regulate dynamically.[23] Since it is more favorable to create conditions that sustain pharmacologically relevant H_2O_2 levels directly at the tumor site,[24] a system capable of *in situ*, electronically tunable peroxide generation could overcome these constraints.

We propose an electrochemical method for *in situ* production of H_2O_2 by reduction of the dissolved oxygen. This approach allows local, continuous peroxide production controlled electronically through the applied current or potential. The concept fits within the broader family of electricity-assisted cancer therapies, which use electrical energy to modulate biological responses.[25] Conventional electrotherapies encompass several distinct modalities. Electrosurgery removes tissue by Joule heating but lacks selectivity.[26] Irreversible electroporation (IRE) kills cells by permeabilizing their membranes using short, high-voltage pulses, though precise control often requires complex modeling of the electric field distribution.[25,27] Tumor-treating fields apply high-frequency alternating currents to interfere with cell division, though the mechanism is not fully understood and the therapeutic utility is limited to brain cancers.[25] Electrochemical treatment (EChT) instead applies direct current to drive water electrolysis in the tumor, creating extreme pH shifts that ablate both healthy and cancerous tissue.[28] In contrast, our approach retains the spatial precision of electrode-based methods but replaces destructive electrolysis with currents 10–100 times lower than those previously employed in EChT. These lower currents support the two-electron oxygen reduction reaction (ORR), which entails the electrochemical reduction of dissolved oxygen to generate pharmacological levels of hydrogen peroxide:

$$O_2 + 2\,H^+ + 2\,e^- \rightarrow H_2O_2 \qquad (R1)$$

This reaction depends on dissolved O_2 in the surrounding medium or tissue. While oxygenation levels in tissue vary greatly,[29] and tumor tissue can be particularly hypoxic,[30]

 This journal is © The Royal Society of Chemistry 2025

Open Access Article. Published on 09 December 2025. Downloaded on 1/18/2026 3:46:00 AM. This article is licensed under a Creative Commons Attribution 3.0 Unported Licence.

dissolved oxygen is usually available at sufficient levels to support this reaction.[31] Thermodynamically, however, ORR more readily proceeds *via* the 4-electron reduction to water, Reaction (R2)):

$$O_2 + 4\ H^+ + 4\ e^- \rightarrow 2\ H_2O \quad (R2)$$

Moreover, the 2-electron reduction of peroxide further to water (Reaction (R3)) is also thermodynamically more favored than Reaction (R1).

$$H_2O_2 + 2\ H^+ + 2\ e^- \rightarrow 2\ H_2O \quad (R3)$$

Electrocatalysts capable of promoting Reaction (R1) while suppressing Reactions (R2) and (R3) are therefore crucial for stable peroxide accumulation.[32,33] Although extensively studied in energy and sustainable chemistry,[33–35] such catalytic systems remain largely unexplored in biological contexts.[36–38]

To address this, we systematically evaluated electrode materials (Fig. 1(f)) and electrochemical conditions to achieve efficient, selective, and reproducible peroxide generation in biological media. Building on these findings, we developed a scalable, eight-channel electrochemical platform compatible with standard 96-well plates, enabling parallel *in situ* peroxide generation and control across multiple wells (Fig. 1(d)–(g)). This platform serves as a proof of concept for tunable peroxide delivery in controlled *in vitro* environments. To validate its biological relevance, we applied it to two cancer cell lines: A375 melanoma and U87 glioblastoma that exhibit distinct peroxide sensitivities (Fig. 1(c)), demonstrating hydrogen peroxide-induced cell death consistent with their redox characteristics.[17]

2. Materials and methods

2.1. Electrode fabrication

The working electrodes (WE) were shaped into a spiral from a 0.6 mm diameter – Au (>99.99%, redox.me) and stainless steel (316L) or 0.8 mm diameter Ti (99.6%, Cetima) wires to produce ~0.7 cm^2 active area when submerged into a 96-well cell culture plate filled with 250 μL electrolyte. The electrodes were cathodically cleaned for 10 min in 1 M NaOH until hydrogen evolution reaction (HER) was clearly visible. The PEDOT electrodes were produced by dip coating of a Ti wire in poly(3,4-ethylenedioxythiophene):polystyrene sulfonate (PEDOT:PSS). The cleaned Ti wire was etched in a solution of $HF:H_2O_2:H_2O$ (1 : 1 : 37.5) for 4 min, washed in deionized water, and exposed to 0.1 M NaOH for 30 s to grow a uniform oxide layer. Immediately after, the electrodes were dip coated with PEDOT:PSS mixture – Clevios™ PH 1000 (Heraeus Holding GmbH), 5 wt% dimethyl sulfoxide (DMSO, Sigma Aldrich), 0.1 wt% dodecyl benzene sulfonic acid (DBSA, Sigma Aldrich), and 2 wt% of (3-glycidyloxypropyl)-trimethoxysilane (GOPS, Sigma Aldrich) filtered through a 0.45 μm PVDF membrane filter. The electrodes were then annealed in an oven at 130 °C for 1 hour. Finally, the PEDOT electrodes were washed in deionized water overnight. The counter electrodes (CE) were made of Ti wire (0.4 mm diameter, 2.3 cm^2) and cleaned cathodically. Reference electrodes were Ag/AgCl wires.

2.2. Multi-channel electrochemical platform fabrication

The body of the platform was machined from Delrin (Polyoxymethylene) high-performance plastic material (Tribon s.r.o.) using our in-house CNC router. Electrical connections to all electrodes were established *via* a custom printed circuit board (PCB) manufactured by JLCPCB.com. The PCB was equipped with screw terminals to connect all electrodes, which were cut to size and shaped manually using pliers. The body of the platform and the PCB were assembled using nylon screws, and the gap between them was filled with PDMS elastomer (Sylgard™ 170). Salt bridges were cut to shape from cleanroom wipes and inserted into machined slots in the body of the platform. These slots were then covered by custom 3D-printed polypropylene plugs to prevent the salt bridges from drying out. The entire platform was connected by a flat ribbon cable to male pin connectors on the PCB, which interfaced with a second custom PCB. This second PCB served as an interface between the 4 mm banana connectors from the 8-channel potentiostat and the platform.

2.3. Electrode characterization

The electrodes were characterized in an H-cell format using the custom built 8-channel integrated platform with an 8-channel potentiostat (OctoStat200, Ivium Technologies). Two neighboring wells of a 96-well plate were used as separate compartments, which were connected by salt bridges made of a cleanroom wipe (2 × 30 mm stripe, 55% cellulose, 45% polyester, KaliWipe). All characterization experiments were done at 37 °C. The salt bridges were changed after each measurement. Between experiments, the platforms were washed in deionized water. The WE compartment was filled with either phosphate buffer saline (PBS) or FluoroBrite™ DMEM (Gibco™, USA) supplemented with 10% active FBS (Gibco™, USA) and 1% Penicillin–Streptomycin (PS, Gibco™, USA), the CE compartment was filled with PBS. After the electrochemical treatment, an aliquot of the WE electrolyte was taken for determination of produced H_2O_2. The H_2O_2 concentration was determined using a horseradish peroxidase (HRP, Sigma Aldrich) and 3,3′,5,5′-tetramethylbenzidine (TMB, Sigma Aldrich) assay, with absorbance measured on a Synergy H1 plate reader (Agilent). The assay mixture consisted of 993 μL citrate–phosphate buffer (pH 5.7), 5 μL TMB (10 mg mL^{-1} in DMSO), and 2 μL HRP (89.9 U mg^{-1}, 1 mg mL^{-1} in H_2O). An aliquot of the treated sample was mixed with the experimental medium (PBS or FluoroBrite/FBS/PS) to a final volume of 100 μL, to which 100 μL of the assay mixture was added. For samples prepared in PBS, absorbance was read at 653 nm, as the signal remained stable over time. However, in the cell culture medium, the absorbance at 653 nm dropped significantly over time due to the processing of H_2O_2 by FBS. To stabilize the TMB product in these conditions, 100 μL of 1 M H_2SO_4 was added, converting the reaction product to its yellow diimine form, which was then read at 450 nm. While the 450 nm signal was more stable, the timing of the assay was precisely controlled and aligned with the calibration curves to

Open Access Article. Published on 09 December 2025. Downloaded on 1/18/2026 3:46:00 AM. This article is licensed under a Creative Commons Attribution 3.0 Unported Licence.

ensure consistency and comparability. Calibration curves were prepared in the respective medium using a 30% H_2O_2 solution (Sigma Aldrich), and sample concentrations were interpolated accordingly. All data are presented as mean ± standard deviation (SD).

2.4. H_2O_2 scavenging assay

The stability of externally added H_2O_2 was evaluated in FluoroBrite DMEM, in FluoroBrite supplemented with 1% penicillin–streptomycin and 10% heat-inactivated FBS (Gibco™, referred to as FluoroBrite + hiFBS), and in FluoroBrite supplemented with 1% penicillin–streptomycin and 10% active FBS (Gibco™, referred to as FluoroBrite + FBS). H_2O_2 was added at initial concentrations of 200 μM, 100 μM, or 50 μM, and aliquots were collected over 40 min for quantification using the HRP/TMB assay described above.

2.5. Cell culture

The human glioblastoma cell line U87 and the human melanoma cell line A375 (both provided by MUG cell bank) were cultured at 37 °C and 5% CO_2. The U87 cell line was cultivated in Eagle's minimum essential medium (E-MEM, Sigma-Aldrich, USA, Catalog Nr. M2279) supplemented with 2 mM L-glutamine, 0.1 mM non-essential amino acids (NEAA), and 10% FBS. The A375 cell was cultivated in Dulbecco's Modified Eagle's Medium – high glucose (D-MEM, Sigma-Aldrich, USA, Catalog Nr. D6429) supplemented with 10% FBS. Cells were cultured in tissue culture flasks with canted neck and filter caps for adherent cells (Sarstedt AG & Co. KG, Germany). Media was changed every 3–4 days, and splitting was performed at ~80% confluency in a 1 : 4 ratio. For cell splitting, cells were detached with TrypLE Express (Gibco, Denmark) and counting was performed using a LUNA-II™ Automated Cell Counter (Logos biosystems, South Korea).

2.6. Manual determination of IC_{50} of H_2O_2

For the manual peroxide treatment, 20 000 cells in 100 μL FluoroBrite + FBS per well were seeded into flat-bottom, black 96-well plates (Corning®, USA). Treatment with H_2O_2 was performed 24 h after seeding with varying concentrations of H_2O_2 (Sigma-Aldrich, USA) ranging from 25–1000 μM H_2O_2. Analysis of cell viability was carried out using the PrestoBlue™ cell viability assay (Invitrogen, USA) 24 h after the peroxide addition. After aspirating the medium of each well, 100 μL of a 1 : 10 dilution of the PrestoBlue™ reagent with FluoroBrite + FBS was added to each well and fluorescence was measured at excitation 540–570 nm and emission 580–610 nm after 2 h of incubation with the PrestoBlue™ reagent using a CLARIOstar Plus plate reader (BMG LABTECH, Germany). IC_{50} values were obtained by fitting data points to a sigmoidal curve using Prism 9 software (GraphPad, USA) and the following equation, in which top and bottom refers to the minimally and maximally inhibited response, respectively:

$$y = \text{Bottom} + \frac{\text{Top} - \text{Bottom}}{1 + \left(\frac{IC_{50}}{x}\right)^{\text{Hill}}} \quad (1)$$

2.7. Galvanostatic H_2O_2 treatment with PEDOT electrodes

The cell culture electrochemical treatment was performed without a RE in a 2-electrode setup. The electrochemical platforms were UV-sterilized prior use. Between separate experiments, the platforms were sterilized by dipping in 70% EtOH for 1 min followed by 3 washes in sterile water. The salt bridges were autoclaved and exchanged before each experiment. Galvanostatic peroxide treatment was done for longer treatment times for the more robust U87 glioblastoma cell line (30/60/90/180 min) and for shorter treatment times for the more sensitive A375 melanoma cell line (5/10/15/20/25/30 min). 20 000 cells were plated in flat bottom, black 96-well plates (Corning®, USA) in 250 μL FluoroBrite + FBS. The galvanostatic treatment was performed 24 h after seeding. 1 μM staurosporine (Sigma Aldrich, USA), acting as a positive apoptosis control, was added immediately before the galvanostatic treatment. For the catalase experiments, a stock solution of catalase from bovine liver (batch No. SLCQ6569, 3291 U mg^{-1} protein; Sigma Aldrich, USA) was freshly prepared and sterile filtered with syringe filters (0.2 μm cellulose acetate, VWR, USA) and added to the culture medium at a final activity of 200 U mL^{-1} just before the treatment. PrestoBlue assay and sigmoidal fit was performed as described above.

3. Results and discussion

3.1. Integrated electrochemical platform

To facilitate the electrochemical characterization and later the delivery of H_2O_2 to cultured cells, we designed an innovative platform compatible with standard 96-well plates. This integrated platform replaces the traditional lid, incorporating all necessary components for the electrochemical cell: working electrode (WE), reference electrode (RE), counter electrode (CE), and salt bridge. These components are introduced from the top and inserted into the plate wells filled with electrolyte or cell culture medium. We selected metal wires as the electrode material, allowing for easy exchange and versatility. The platform employs an H-cell configuration where two neighboring wells serve as separate compartments of the electrochemical cell (Fig. 1(e)). These are electrolytically connected using an interchangeable salt bridge, ensuring efficient ion exchange between the compartments. The electronic connections are seamlessly integrated within the platform, facilitating a tidy and efficient link to an 8-channel potentiostat, enabling the simultaneous treatment of eight electrochemical cells (Fig. 1(g) and SI, Fig. S1). This design not only enhances the throughput of the electrochemical treatments but also ensures consistent and reproducible delivery of H_2O_2 across multiple wells.

3.2. Characterization of electrode materials for H_2O_2 production

While electrocatalysts for sustained hydrogen peroxide production *via* ORR have been explored in detail for industrial applications, usually under alkaline conditions, studying continuous hydrogen peroxide generation in a biological environment is rare. To find a

 This journal is © The Royal Society of Chemistry 2025

Open Access Article. Published on 09 December 2025. Downloaded on 1/18/2026 3:46:00 AM. This article is licensed under a Creative Commons Attribution 3.0 Unported Licence.

system for on-demand hydrogen peroxide evolution in cell culture conditions, we initiated the characterization process using well-known materials that support the oxygen reduction reaction (ORR, Reaction (R1)) to hydrogen peroxide: gold (Au)[39] and 316L grade stainless steel.[36,40] Both materials were able to produce approximately 50 μM H_2O_2 concentration in phosphate-buffered saline (PBS) after 10 minutes at their optimal potentials (Fig. 2(a)). However, significant conditioning behavior was observed with these materials, where the efficiency of hydrogen peroxide production depended on the history of the electrode until a semi-stable condition was reached (SI, Fig. S2). Furthermore, both materials exhibited high variability between electrodes when used in cell culture medium (Fig. 2(b)).

In light of these challenges, we explored another known electrocatalyst: poly(3,4-ethylenedioxythiophene):polystyrene sulfonate (PEDOT) coating.[41,42] Titanium wire was used as a support due to its excellent interface with PEDOT, its ability to support hydrogen peroxide production at slightly higher potentials than PEDOT, and its relatively high overpotential for hydrogen evolution reaction (which typically causes PEDOT delamination). To promote PEDOT adhesion, the Ti wire was partially etched to create a clean and roughened surface.

PEDOT electrodes produced higher hydrogen peroxide concentrations in both PBS and the cell culture medium, with a much narrower distribution than gold or steel (Fig. 2(a) and (b)). PEDOT electrodes in galvanostatic condition (−7 μA, −10 μA cm^{-2}) turned out to be the most reproducible choice for prolonged use in cell culture medium. This configuration showed tight distribution across all electrodes and the highest accumulated amount of hydrogen peroxide (Fig. 2(c)). Galvanostatic measurements also showed that PEDOT exhibits the highest faradaic efficiency of all tested materials (SI, Fig. S3). Interestingly, PEDOT exhibited essentially no conditioning effect, as long as it was hydrated before operation. Four different sets of eight electrodes performed identically, even when one of the platforms was extensively used in cell culture experiments for a week (20 h total runtime) and then characterized along with the pristine ones (Fig. 2(d)).

Therefore, galvanostatic operation of PEDOT electrodes was chosen as the optimal condition. We demonstrated that the amount of *in situ* formed H_2O_2 could be controlled by the applied current and time. Generally, increasing the current results in higher hydrogen peroxide production, which is more pronounced in PBS compared to the culture medium (Fig. 2(e)).

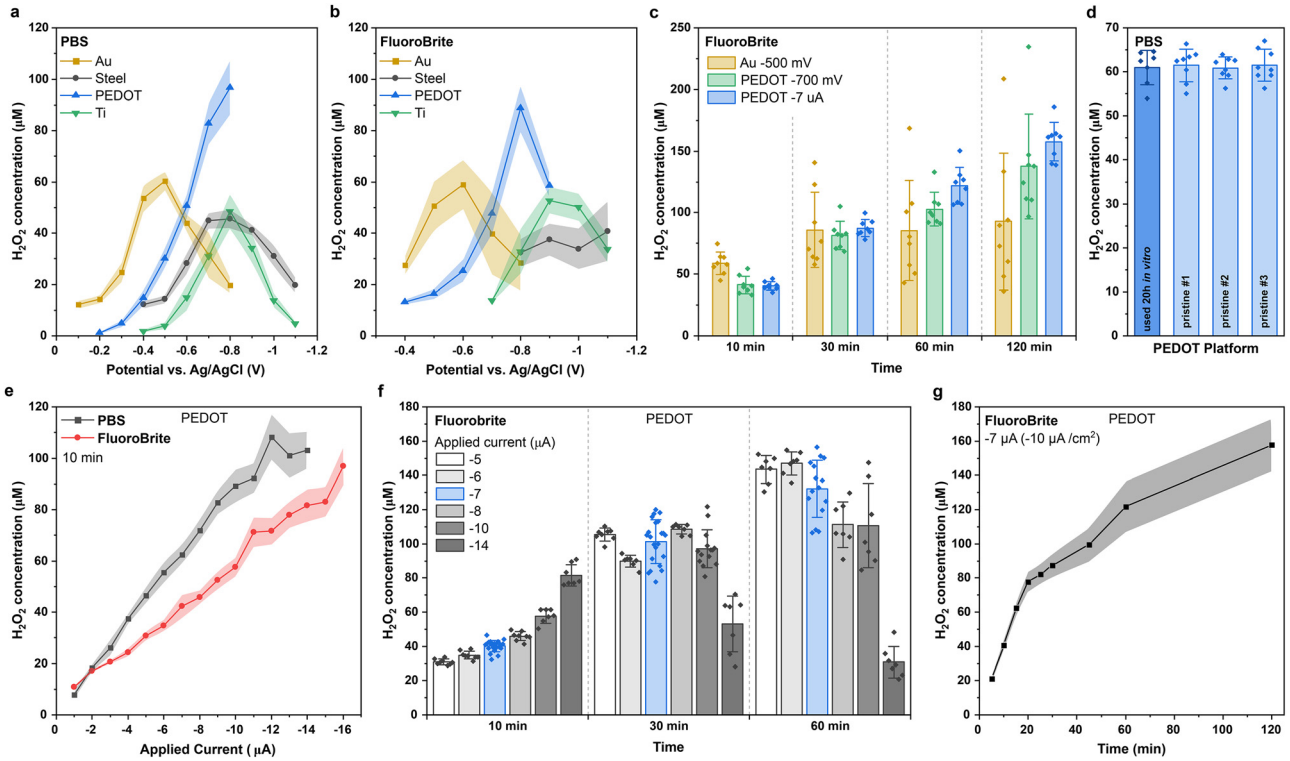

Fig. 2 Optimization of hydrogen peroxide generation by ORR. (a), (b) Hydrogen peroxide concentration as a function of potential applied for 10 minutes in (a) PBS and (b) FluoroBrite medium. PEDOT exhibits optimal H_2O_2 generation in both PBS and the medium. (c) Comparison of potentiostatic and galvanostatic H_2O_2 generation at different time intervals using PEDOT and Au electrodes in FluoroBrite + FBS, −7 μA ≙ −10 μA cm^{-2}. (d) Reproducibility of galvanostatic H_2O_2 generation (10 min run) using PEDOT across four different platforms, including a platform previously used for *in vitro* cellular experiments over the course of a week (total run time 20 h). (e) Comparison of H_2O_2 concentrations achieved after 10 minutes of operation in PBS *versus* FluoroBrite + FBS, as a function of applied galvanostatic current (electrode area = 0.7 cm^2). (f) For short treatment times (10 min), higher currents result in elevated H_2O_2 production, while for longer treatments (30 to 60 min), lower currents (−5 to −7 μA) maintain higher and consistent H_2O_2 levels. (g) H_2O_2 production over time in FluoroBrite + FBS medium under constant application of −7 μA ≙ −10 μA cm^{-2}. For panels a, b, e, and g, the data represent the mean ± SD ($n \geq 8$).

Open Access Article. Published on 09 December 2025. Downloaded on 1/18/2026 3:46:00 AM.
This article is licensed under a Creative Commons Attribution 3.0 Unported Licence.

This difference is attributed to the culture medium containing enzymatically active fetal bovine serum (FBS), which rapidly clears the hydrogen peroxide (Fig. 1(b)) *via* catalase and peroxidase activity.[43] To directly assess the scavenging properties of the medium, we monitored the stability of added hydrogen peroxide in pure FluoroBrite, in medium supplemented with heat-inactivated FBS, and in medium with active FBS (SI, Fig. S4). These measurements confirmed that enzymatic activity in serum is the dominant contributor to peroxide clearance. Notably, all peroxide generation and *in vitro* experiments in this study were conducted using active FBS, representing a worst-case scavenging scenario. For longer operation times, where oxygen concentration and reaction equilibrium are limiting factors, a lower current density is optimal to prevent the competing reduction reaction (Reaction (R3)) of accumulated hydrogen peroxide to water (Fig. 2(f)). For extended run times, −7 μA (−10 μA cm^{-2}) was found to be the optimal current (current density) to ensure continuous accumulation of hydrogen peroxide (Fig. 2(g)).

3.3. Cathodic PEDOT operation produces pharmacologically relevant H_2O_2 concentrations and induces cancer cell death *in vitro*

We evaluated the cytotoxic properties of our H_2O_2 generating platform on two human cancer cell lines: the H_2O_2-sensitive melanoma A375 and the more resilient glioblastoma U87, as shown by our data (Fig. 1(c)) and supported by the literature.[17] The PEDOT platform (Fig. 1(f)) was inserted into 96-well plates containing 20 000 cells per well in FluoroBrite + FBS medium (Fig. 1(e)) and operated galvanostatically at −7 μA (−10 μA cm^{-2}) for various durations. Cell viability was assessed 24 hours post-treatment (Fig. 3(a) and (b)). A 30-minute treatment induced complete cell death in A375 cells (Fig. 3(b)), while U87 cells required a 90-minute treatment to achieve a similar effect (Fig. 3(b)). As shown in Fig. 2(f), the platform produced an H_2O_2 concentration of approximately 80 μM after 30 minutes of operation. This resulted in near-complete cell death for the sensitive A375 cell line. In contrast, manual treatment with 80 μM H_2O_2 led to approximately 25% viability for A375 cells (Fig. 1(c)), suggesting that our platform's continuous H_2O_2 delivery outperforms manual treatment. This advantage likely stems from the rapid degradation of H_2O_2 in the manual treatment, highlighting the efficiency of our system in maintaining effective cytotoxic concentrations. A sham control using the same setup without electrical addressing showed no impact on cell viability (SI, Fig. S5).

To confirm that the observed cytotoxicity was solely due to the *in situ* generation of H_2O_2 and not other electrochemical factors such as the electric field, oxygen depletion, or pH changes, we added catalase to the cell culture medium before operating the PEDOT electrodes. Catalase addition fully protected the cells during the previously lethal treatment times: 30 minutes for A375 (Fig. 3(c)) and 90 to 180 minutes for U87 (Fig. 3(d)). Interestingly, U87 cells were completely unaffected at the 90-minute treatment when catalase was present. However, a slight reduction

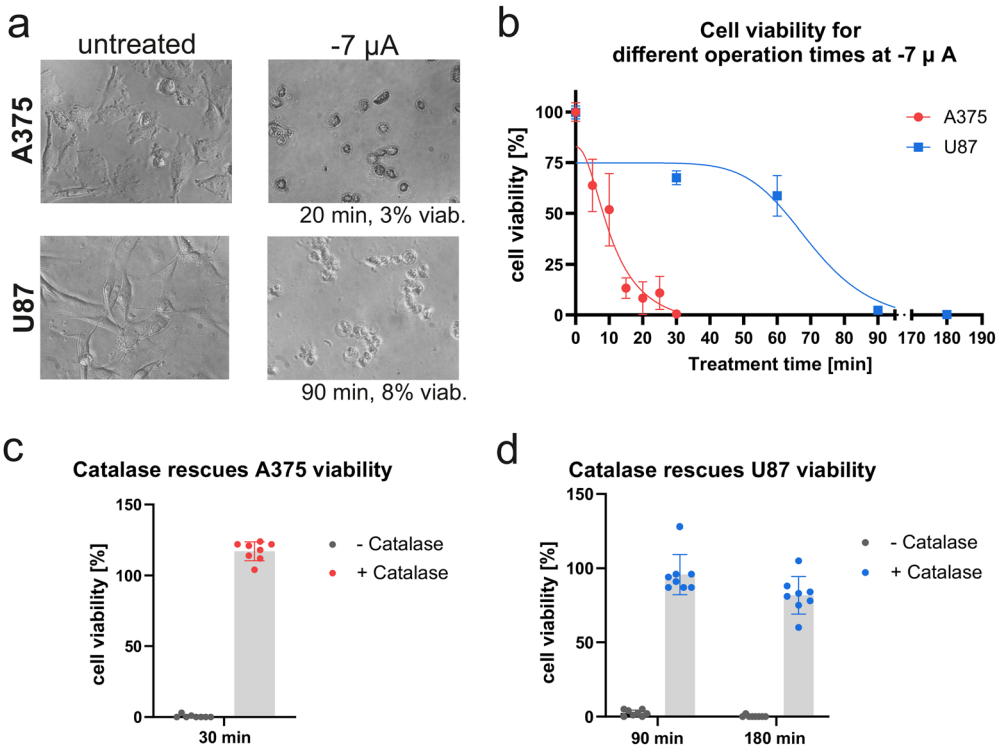

Fig. 3 Effect of cathodic PEDOT treatment on cell viability. (a) Representative microscopic images of A375 and U87 cells, untreated (left panel) and 24 h post-cathodic PEDOT treatment at −7 μA for 20 min (A375) and 90 min (U87). Percent viability is indicated. (b) Quantitative cell viability of A375 and U87 cells at different durations of cathodic PEDOT treatment (−7 μA ≙ −10 μA cm^{-2}), showing time-dependent decreases in viability. (c), (d) Catalase (200 U mL^{-1}) present during cathodic PEDOT treatment preserves cell viability in A375 (c) and U87 (d) cells, mitigating H_2O_2-induced cytotoxicity.

This journal is © The Royal Society of Chemistry 2025

Open Access Article. Published on 09 December 2025. Downloaded on 1/18/2026 3:46:00 AM. This article is licensed under a Creative Commons Attribution 3.0 Unported Licence.

in cell viability was observed at the 180-minute mark, suggesting H_2O_2-independent cell death. Thus, for prolonged treatments, it is crucial to determine the optimal galvanostatic current to produce H_2O_2 (Fig. 2(f)).

4. Conclusions

The use of H_2O_2 in cancer treatment was first explored by Linus Pauling and Ewan Cameron in 1975, when they administered high doses of intravenous vitamin C (a pro-drug for H_2O_2) to late-stage cancer patients.[44] Their findings demonstrated an increase in median survival from 50 to 210 days. However, despite the extensive number of clinical trials conducted since then—currently over 600 trials involving vitamin C in cancer therapy are registered (clinicaltrials.gov)—the challenge remains in maintaining sufficiently high, localized concentrations of H_2O_2 for effective treatment. Indeed, a recent clinical study has shown that dosing ascorbate three times a week to metastatic pancreatic cancer patients doubles survival time, strongly hinting towards improved effects when the H_2O_2 treatment is more frequent.[24] Our study addresses this limitation by developing a continuous hydrogen peroxide generating system, converting dissolved oxygen into H_2O_2 *via* a simple electrocatalytic mechanism.

In contrast to existing electrochemical therapies that utilize much higher current densities >0.5 mA cm^{-2} which achieve their effects through water electrolysis,[28] our system operates at lower currents, specifically $\sim$10 μA cm^{-2}. This controlled application allows for more precise targeting of tumor cells while reducing potential damage to surrounding healthy tissues. Achieving consistent H_2O_2 production required optimizing the ORR in biological media, a task we found non-trivial – particularly as all experiments were conducted in medium supplemented with active FBS, intentionally chosen to approximate *in vivo*-like enzymatic scavenging and represent a worst-case scenario for peroxide stability. After evaluating several materials, including gold and stainless steel, we identified PEDOT as a highly stable and reproducible electrocatalyst for generating pharmacologically relevant concentrations of H_2O_2 in biological conditions, sufficient to induce cancer cell death.

Our data confirm that the produced H_2O_2 induces effective cell death in both highly sensitive and robust cancer cell lines. It is known that peroxide can induce cell death through multiple mechanisms, broadly apoptosis is triggered by moderate H_2O_2 levels and necrosis occurs at higher concentrations. Moreover, oxidative stress, driven by excess ROS like H_2O_2, is known to play a crucial role in various forms of regulated cell death beyond apoptosis. One of the most prominent examples is ferroptosis, an iron-dependent form of cell death marked by the accumulation of lipid peroxides and distinct from both apoptosis and necrosis.[45] Given that ferroptosis is also regulated by oxidative stress, it is possible that the H_2O_2 levels in our experiments may trigger this pathway under certain conditions, especially in cancer cells with high iron content or dysregulated antioxidant defenses.[46] To fully unravel the contribution of different death pathways—apoptosis, necrosis, or ferroptosis—more detailed studies using molecular biology techniques will be necessary.[47]

This study was focused on developing and optimizing a multielectrode platform for *in vitro* experiments, enabling systematic evaluation of electrode materials and protocols in cell culture plates. At the same time, we believe that the principles demonstrated here can inform future *in vivo* applications. Recent advances in PEDOT-based bioelectronics already support a variety of form factors, including large-area flexible arrays, microneedles, catheters, and microelectrodes.[48] Building on these developments, we envision flexible implantable peroxide-generating electrodes positioned at tumor resection margins, or coatings applied to established electrode technologies such as stereoelectroencephalography (SEEG) or deep brain stimulation (DBS) electrodes for brain tumor applications. These possibilities are exploratory, but they illustrate how continuous electrochemical peroxide delivery could eventually be adapted beyond the *in vitro* context.

Further, while our results in 2D cell cultures offer valuable insights into H_2O_2 sensitivity, translating this technology to *in vivo* applications introduces challenges, particularly regarding oxygen availability. Physiological oxygen levels vary widely across tissues, with tumor regions often exhibiting severe hypoxia due to disorganized vasculature.[29,30] This variability in oxygenation, even within a single tumor, poses potential barriers to the effectiveness of our therapy. However, this hypoxic tumor microenvironment may also present an opportunity: exacerbating oxygen deprivation in already hypoxic tumor regions could be combined with hypoxia-activated prodrugs,[49,50] amplifying the stress induced by H_2O_2. Alternatively, targeting the normoxic tumor periphery, where H_2O_2 production is more efficient, could initiate cell death at the margins, and prevent tumor outgrowth into healthy tissue. In addition, localized electrochemical peroxide delivery may be particularly useful in post-resection therapy, where oxygen supply is less restricted and local control at surgical margins is critical to prevent recurrence. Tumor response to peroxide is also expected to vary with redox phenotype, including differences in catalase and peroxidase activity. As highlighted by Doskey *et al.*,[17] tumor cells differ widely in their ability to metabolize H_2O_2, which strongly influences therapeutic efficacy. This heterogeneity suggests that peroxide-based approaches may be most effective in a personalized framework, where tumor responsiveness is assessed using patient-derived models or biomarker analysis.

Author contributions

M. J.: conceptualization, supervision, methodology, electrode fabrication, electrochemical characterization, writing – original draft, writing – review and editing. L. W.: supervision, funding acquisition, methodology, writing – original draft, writing – review and editing. J. E.: platform design and fabrication, hardware for *in vitro* investigation. S. E.: *in vitro* investigation and validation. L. N. and V. H.: *in vitro* investigation and

validation. E. D. G.: conceptualization, supervision, funding acquisition, writing – review and editing.

Conflicts of interest

The authors from Brno University of Technology (MJ, JE, and EDG) are working towards commercializing the multichannel electrochemical platform used for the *in vitro* experiments described in this manuscript.

Data availability

All data used in this work are available on Figshare at https://figshare.com/s/404786d9f9a038600988.

The data supporting this article have been included as part of the supplementary information (SI). Supplementary information is available. See DOI: https://doi.org/10.1039/d5tb01244a.

Acknowledgements

The work was supported from the Grant Agency of the Czech Republic: Faraday Scalpel: precision ablation of the brain tissue by electrochemical reduction of oxygen (no 23-07432S). Sample fabrication was made possible by CzechNanoLab Research Infrastructure supported by MEYS CR (LM2023051). Collaboration between the Brno and Graz teams was supported by a bilateral travel grant MEYS CR 8J23AT001. Support was also provided by BioTechMed Graz *via* a Young Research Groups project grant, and the European Union's Horizon Europe program *via* the EIC Pathfinder Open project 101099963.

References

1 Y. Saito, K. Nishio, Y. Ogawa, J. Kimata, T. Kinumi, Y. Yoshida, N. Noguchi and E. Niki, *Free Radic Res*, 2006, **40**, 619–630.
2 M. Tochigi, T. Inoue, M. Suzuki-karasaki, T. Ochiai, C. Ra and Y. Suzuki-karasaki, *Int. J. Oncol.*, 2013, **42**, 863–872.
3 A. Nogueira-Pedro, T. A. M. Cesário, C. C. Dias, C. S. T. Origassa, L. P. M. Eça, E. J. Paredes-Gamero and A. T. Ferreira, *Cancer Cell Int.*, 2013, **13**, 1–9.
4 L. Ma, W.-Z. Zhu, T.-T. Liu, H.-L. Fu, Z.-J. Liu, B.-W. Yang, T.-Y. Song and G.-R. Li, *Asian Pac. J. Cancer Prev.*, 2015, **16**, 1637–1642.
5 G. Vilema-Enríquez, A. Arroyo, M. Grijalva, R. I. Amador-Zafra and J. Camacho, *Oxid. Med. Cell. Longevity*, 2016, **2016**, 1908164.
6 W. H. Park, *Oncol. Rep.*, 2018, **40**, 1787–1794.
7 H. Sies, *Redox Biol.*, 2017, **11**, 613–619.
8 K. J. A. Davies, *IUBMB Life*, 1999, **48**, 41–47.
9 Y. Chen, X. Guo, Y. Zeng, X. Mo, S. Hong, H. He, J. Li, S. Fatima and Q. Liu, *Sci. Rep.*, 2023, **13**, 1–14.
10 Z. Shen, J. Song, B. C. Yung, Z. Zhou, A. Wu and X. Chen, *Adv. Mater.*, 2018, **30**, 1704007.
11 J. Xiang, C. Wan, R. Guo and D. Guo, *BioMed Res. Int.*, 2016, **2016**, 7343965.
12 J. D. Schoenfeld, Z. A. Sibenaller, K. A. Mapuskar, B. A. Wagner, K. L. Cramer-Morales, M. Furqan, S. Sandhu, T. L. Carlisle, M. C. Smith, T. Abu Hejleh, D. J. Berg, J. Zhang, J. Keech, K. R. Parekh, S. Bhatia, V. Monga, K. L. Bodeker, L. Ahmann, S. Vollstedt, H. Brown, E. P. Shanahan Kauffman, M. E. Schall, R. J. Hohl, G. H. Clamon, J. D. Greenlee, M. A. Howard, M. K. Shultz, B. J. Smith, D. P. Riley, F. E. Domann, J. J. Cullen, G. R. Buettner, J. M. Buatti, D. R. Spitz and B. G. Allen, *Cancer Cell*, 2017, **31**, 487–500.
13 B. Ngo, J. M. Van Riper, L. C. Cantley and J. Yun, *Nat. Rev. Cancer*, 2019, **19**, 271–282.
14 S. V. Torti and F. M. Torti, *Nat. Rev. Cancer*, 2013, **13**, 342–355.
15 T. Ali, D. Li, T. Nimasha, F. Ponnamperumage, A. K. Peterson, J. Pandey, K. Fatima, J. Brzezinski, J. Anna, R. Jakusz, H. Gao, G. E. Koelsch, D. S. Murugan and X. Peng, *Cancers*, 2024, **16**, 2171.
16 Z. Tang, Y. Liu, M. He and W. Bu, *Angew. Chem., Int. Ed.*, 2019, **131**, 958–968.
17 C. M. Doskey, V. Buranasudja, B. A. Wagner, J. G. Wilkes, J. Du, J. J. Cullen and G. R. Buettner, *Redox Biol.*, 2016, **10**, 274–284.
18 Q. Chen, M. G. Espey, A. Y. Sun, J. H. Lee, M. C. Krishna, E. Shacter, P. L. Choyke, C. Pooput, K. L. Kirk, G. R. Buettner and M. Levine, *Proc. Natl. Acad. Sci. U. S. A.*, 2007, **104**, 8749–8754.
19 Z. Chu, J. Yang, W. Zheng, J. Sun, W. Wang and H. Qian, *Coord. Chem. Rev.*, 2023, **481**, 215049.
20 Y. Deng, S. Huang, G. Jiang, L. Zhou, A. Nezamzadeh-Ejhieh, J. Liu and Z. Zhou, *RSC Med. Chem.*, 2024, **15**, 2996–3016.
21 F. Böttger, A. Vallés-Martí, L. Cahn and C. R. Jimenez, *J. Exp. Clin. Cancer Res.*, 2021, **40**, 1–44.
22 J. González-Montero, S. Chichiarelli, M. Eufemi, F. Altieri, L. Saso and R. Rodrigo, *Molecules*, 2022, **27**, 1–20.
23 Q. Chen, M. G. Espey, M. C. Krishna, J. B. Mitchell, C. P. Corpe, G. R. Buettner, E. Shaded and M. Levine, *Proc. Natl. Acad. Sci. U. S. A.*, 2005, **102**, 13604–13609.
24 K. L. Bodeker, B. J. Smith, D. J. Berg, C. Chandrasekharan, S. Sharif, N. Fei, S. Vollstedt, H. Brown, M. Chandler, A. Lorack, S. McMichael, J. Wulfekuhle, B. A. Wagner, G. R. Buettner, B. G. Allen, J. M. Caster, B. Dion, M. Kamgar, J. M. Buatti and J. J. Cullen, *Redox Biol.*, 2024, **77**, 103375.
25 S. Zhong, S. Yao, Q. Zhao, Z. Wang, Z. Liu, L. Li and Z. L. Wang, *Adv. NanoBiomed Res.*, 2023, **3**, 2200143.
26 P. Bourdillon, B. Devaux, A. S. Job-Chapron and J. Isnard, *Neurophysiol. Clin.*, 2018, **48**, 59–64.
27 J. F. Edd, L. Horowitz, R. V. Davalos, L. M. Mir and B. Rubinsky, *IEEE Trans. Biomed. Eng.*, 2006, **53**, 1409–1415.
28 C. O'Brien and A. Ignaszak, *ChemElectroChem*, 2020, **7**, 3895–3904.
29 A. Carreau, B. El Hafny-Rahbi, A. Matejuk, C. Grillon and C. Kieda, *J. Cell. Mol. Med.*, 2011, **15**, 1239–1253.
30 S. R. McKeown, *Br. J. Radiol.*, 2014, **87**, 1–12.

Open Access Article. Published on 09 December 2025. Downloaded on 1/18/2026 3:46:00 AM. This article is licensed under a Creative Commons Attribution 3.0 Unported Licence.

 This journal is © The Royal Society of Chemistry 2025

Open Access Article. Published on 09 December 2025. Downloaded on 1/18/2026 3:46:00 AM.
This article is licensed under a Creative Commons Attribution 3.0 Unported Licence.

31 H. M. Swartz, A. B. Flood, P. E. Schaner, H. Halpern, B. B. Williams, B. W. Pogue, B. Gallez and P. Vaupel, *Physiol. Rep.*, 2020, **8**, e14541.
32 X. Huang, M. Song, J. Zhang, T. Shen, G. Luo and D. Wang, *Nano-Micro Lett.*, 2023, **15**, 86.
33 Y. Bu, Y. Wang, G.-F. Han, Y. Zhao, X. Ge, F. Li, Z. Zhang, Q. Zhong and J.-B. Baek, *Adv. Mater.*, 2022, **2103266**, 1–19.
34 Z. Lu, G. Chen, S. Siahrostami, Z. Chen, K. Liu, J. Xie, L. Liao, T. Wu, D. Lin, Y. Liu, T. F. Jaramillo, J. K. Nørskov and Y. Cui, *Nat. Catal.*, 2018, **1**, 156–162.
35 S. C. Perry, D. Pangotra, L. Vieira, L. I. Csepei, V. Sieber, L. Wang, C. Ponce de León and F. C. Walsh, *Nat. Rev. Chem.*, 2019, **3**, 442–458.
36 O. Istanbullu, J. Babauta, H. D. Nguyen and H. Beyenal, *Biofouling*, 2012, **28**, 769–778.
37 S. T. Sultana, E. Atci, J. T. Babauta, A. Mohamed Falghoush, K. R. Snekvik, D. R. Call and H. Beyenal, *Sci. Rep.*, 2015, **5**, 14908.
38 Y. S. Raval, D. Fleming, A. Mohamed, M. J. Karau, J. N. Mandrekar, A. N. Schuetz, K. E. Greenwood-quaintance, H. Beyenal and R. Patel, *Adv. Ther.*, 2023, **6**, 2300059.
39 E. Miglbauer, O. S. Abdullaeva, M. Gryszel and E. D. Głowacki, *ChemBioChem*, 2023, **24**, 1–13.
40 J. Ehlich, L. Migliaccio, I. Sahalianov, M. Nikic, J. Brodský, I. Gablech, X. T. Vu, S. Ingebrandt and E. D. Glowacki, *J. Neural Eng.*, 2022, **19**, 036045.
41 E. Mitraka, M. Gryszel, M. Vagin, M. J. Jafari, A. Singh, M. Warczak, M. Mitrakas, M. Berggren, T. Ederth, I. Zozoulenko, X. Crispin and E. D. Głowacki, *Adv. Sustainable Syst.*, 2019, **3**, 1800110.
42 O. S. Abdullaeva, I. Sahalianov, M. Silverå Ejneby, M. Jakešová, I. Zozoulenko, S. I. Liin and E. D. Głowacki, *Adv. Sci.*, 2022, **9**, 1–14.
43 D. Boehm, C. Heslin, P. J. Cullen and P. Bourke, *Sci. Rep.*, 2016, **6**, 21464.
44 E. Cameron and L. Pauling, *Proc. Natl. Acad. Sci. U. S. A.*, 1976, **73**, 3685–3689.
45 S. J. Dixon, K. M. Lemberg, M. R. Lamprecht, R. Skouta, E. M. Zaitsev, C. E. Gleason, D. N. Patel, A. J. Bauer, A. M. Cantley, W. S. Yang, B. Morrison and B. R. Stockwell, *Cell*, 2012, **149**, 1060–1072.
46 B. Hassannia, P. Vandenabeele and T. Vanden Berghe, *Cancer Cell*, 2019, **35**, 830–849.
47 Y. Vinik, A. Maimon, V. Dubey, H. Raj, I. Abramovitch, S. Malitsky, M. Itkin, A. Ma'ayan, F. Westermann, E. Gottlieb, E. Ruppin and S. Lev, *Adv. Sci.*, 2024, **11**, 1–21.
48 M. Bianchi, A. De Salvo, M. Asplund, S. Carli, M. Di Lauro, A. Schulze-bonhage, T. Stieglitz, L. Fadiga and F. Biscarini, *Adv. Sci.*, 2022, **9**, 2104701.
49 S. Wan, G. Zhang, R. Liu, M. N. Abbas and H. Cui, *Cell Commun. Signaling*, 2023, **21**, 1–19.
50 J. Huang, P. Yu, M. Liao, X. Dong, J. Xu, J. Ming, D. Bin, Y. Wang, F. Zhang and Y. Xia, *Sci. Adv.*, 2023, **9**, eadf3992.